Science Press

ARTICLE

Effect of Al Addition on Microstructure, Magnetic Properties, and Mechanical Properties of $(Fe_{73}Ga_{27})_{99.8}Tb_{0.2}$ Alloy

Du Jinchao[1,2],   Li Xiaofei[1],   Jiao Peiying[1],   Zhang Zhiguang[1],   Gong Pei[1]

[1] School of Materials Science and Engineering, Inner Mongolia University of Technology, Hohhot 010051, China; [2] Functional Material Research Institute, Central Iron and Steel Research Institute, Beijing 100081, China

Abstract: $(Fe_{73}Ga_{27-x}Al_x)_{99.8}Tb_{0.2}$ (x=0, 1, 2, 3, 4, 5) alloys were prepared by vacuum arc furnace to investigate the effect of Al addition on the microstructure, magnetic properties, and mechanical properties of alloys. Results show that the phase structure of the alloys is still A2 phase and Tb_2Fe_{17} phase, and the metallographic structure is composed of cellular crystal and columnar dendrite. The decrease in lattice constant, the intensification of (100) orientation, and the generation of Tb_2Fe_{17} phase at the grain boundary exert significant effect on the magnetostrictive properties. The fracture morphology of the alloys is intergranular brittle fracture and cleavage fracture, and the causes of fracture occurrence include the segregation of Tb and Al elements. The parallel magnetostrictive strain ($\lambda_{//}$) of $(Fe_{73}Ga_{24}Al_3)_{99.8}Tb_{0.2}$ alloy peaks at 1.04×10^{-4}. It is worth noting that compared with those of $(Fe_{73}Ga_{27})_{99.8}Tb_{0.2}$ alloy, the $\lambda_{//}$ and elongation of $(Fe_{73}Ga_{26}Al_1)_{99.8}Tb_{0.2}$ alloy increase by 18.3% and 53.4%, respectively. Besides, $(Fe_{73}Ga_{26}Al_1)_{99.8}Tb_{0.2}$ alloy possesses the characteristics of high saturation magnetization (M_s), low remanent magnetization (M_r), and coercivity (H_c), which is beneficial to reduce the cost in actual production, but its tensile strength and Vickers hardness decrease to a certain extent. Therefore, the investigation on the micro-mechanism of Al addition on Fe-Ga alloys is of great significance for the development of Fe-Ga alloy devices.

Key words: $(Fe_{73}Ga_{27})_{99.8}Tb_{0.2}$ alloy; Al doping; microstructure; magnetic properties; mechanical properties

Magnetostrictive material is one of the functional metal materials with high application value and wide application range. By mutually converting electromagnetic energy, sound energy, and mechanical energy, the devices, such as brakes, micro-motors, high-power ultrasonic transducers, sensors, micro-displacement actuators, and hydroacoustic transducers, can be manufactured, which are widely applied in military and civilian fields[1–2]. The most extensively studied alloy systems are Tb-Dy-Fe series, whose magnetostrictive strain can reach 1500×10^{-6}–2000×10^{-6} [3–4], but the brittleness, poor mechanical properties, and high cost of Tb and Dy seriously restrict their production. The saturation magnetostrictive strain (λ_s) of Fe-Ga monocrystalline alloys along the easy magnetization direction can achieve 4.00×10^{-4} [5–6], but the high cost, small size, and complex preparation process of single-crystal Fe-Ga alloy restrict its application. Thus, the polycrystalline Fe-Ga materials have been widely researched[7]. Polycrystalline Fe-

Ga alloys have high tensile strength, good machinability, but low saturation magnetostrictive strain. It is shown that doping elements in Fe-Ga alloys can notably affect the magnetic properties and mechanical properties.

The Al element with low cost as well as atomic radius and properties similar to those of Ga element attracts extensive attention as doping element into the Fe-Ga alloys. Mungsantisuk et al[8] argued that the magnetostrictive properties of the alloys did not prominently reduce by adding appropriate Al. Srisukhumbowornchai et al[9] found that the magnetostriction strain of $Fe_{80}Ga_{15}Al_5$ alloy reached 2.34×10^{-4}. Zhou et al[10–11] prepared $Fe_{82}Ga_9Al_9$ alloy and found that its saturation magnetostrictive strain was 8.8×10^{-5} and the magnetostrictive strain increased to 1.14×10^{-4} after magnetic field heat treatment. Li et al[12] found that the saturation magnetostrictive strain of $Fe_{82}Ga_{13.5}Al_{4.5}$ alloy peaked at 2.47×10^{-4}. Moreover, Al can improve the elongation and ductility of

Fe-Ga alloys[13]. Liu et al[14] prepared the rod-like $Fe_{82}Ga_{18-x}Al_x$ (x=0, 4.5, 6, 9, 12, 13.5) alloys by directional solidification method and reported that when the Al content was 4.5at%, the tensile strength and elongation of the alloys reached 492 MPa and 11.4%, respectively, which were higher than those of $Fe_{82}Ga_{18}$ alloy. Nolting et al[15] demonstrated that the addition of Cr, Al, and V elements could improve the elongation and tensile strength of Fe-Ga alloys, and the fracture mode of the alloys was transformed from intergranular fracture to transgranular fracture.

Tb, as one of heavy rare earth elements, has high effective magnetic moment, unique 4f electronic structure, and strong magnetic crystal anisotropy[16–19]. The doping of 0.2at% Tb in Fe-Ga alloys can markedly ameliorate the properties. Zhang et al[20] prepared $Fe_{81}Ga_{19}Tb_x$ (x=0, 0.2, 0.4, 0.6) thin belt by fast hardening and melt-spinning method. The report demonstrated that Tb element was enriched at the grain boundaries and the magnetostrictive strain of $Fe_{81}Ga_{19}Tb_{0.2}$ alloy peaked at $−1.320×10^{-3}$. According to Ref.[21–24], the tensile strength and elongation of $(Fe_{83}Ga_{17})_{99.8}Tb_{0.2}$ alloy reached 595 MPa and 3.5%, respectively, which were significantly higher than those of the undoped alloys. The fracture mode of the alloys changed from intergranular fracture to transgranular fracture and finally to interphase fracture. The dispersed Tb-rich phase greatly increased the dislocation density.

Therefore, $(Fe_{73}Ga_{27})_{99.8}Tb_{0.2}$ alloy was used as matrix in this research and Al element was added to prepare $(Fe_{73}Ga_{27-x}Al_x)_{99.8}Tb_{0.2}$ (x=0, 1, 2, 3, 4, 5) alloys. The effect of Al addition on microstructure, magnetic properties, and mechanical properties of the alloys was investigated.

1　Experiment

Fe, Ga, Al, and Tb metal elements with purity greater than 99.95% were selected as raw materials. Ingredients were designed and calculated based on the composition of $(Fe_{73}Ga_{27-x}Al_x)_{99.8}Tb_{0.2}$ alloys. The total mass of each sample was 80 g.

At the beginning, the weighed samples were placed into a water-cooled copper crucible in a non-consumable vacuum arc furnace. Subsequently, the mechanical pump and pre-extraction valve were turned on to control the air pressure below 5 Pa. Then, the forward valve, gate valve, and high vacuum molecular pump were sequentially switched on to control the air pressure under $5×10^{-2}$ Pa. Next, the high vacuum molecular pump, gate valve, forward valve, and mechanical pump was switched off in sequence and the furnace was filled with high-purity argon gas three times. After the melting process, the ingot was flipped and the melting was repeated three times to ensure uniform alloy composition and good morphology, therefore reducing the structural defects, such as porosity and shrinkage. When the ingot was cooled in a water-cooled copper crucible, undercooling occurred in the longitudinal direction, and the grains grew along this direction. The preferred orientation of the grains significantly exerted the impact on the magnetostrictive performance of the alloys. In consequence,

the sample were obtained by cutting along the longitudinal direction. The sampling position of alloys is shown in Fig. 1. In this research, scanning electron microscope (SEM), energy dispersive spectrometer (EDS), and X-ray diffractometer (XRD) were used for analysis.

2　Results and Discussion

2.1　XRD analysis

Fig. 2 shows XRD patterns of $(Fe_{73}Ga_{27-x}Al_x)_{99.8}Tb_{0.2}$ alloys and Table 1 displays XRD analysis results of 2θ of (100) peak ($2\theta_{100}$), lattice constant a, and I_{200}/I_{110} ratio. As shown in Fig. 2, the characteristic diffraction peaks of the alloys with Al addition are composed of (110), (200), and (211) diffraction peaks, which indicates that the phase structure of the alloys is dominated by the A2 phase. Since the atomic radius of Tb (0.251 nm) is much larger than that of Fe (0.126 nm) and Ga (0.140 nm), Tb can hardly dissolve in the Fe-Ga solid solution. Based on EDS analysis results, Tb is mainly gathered at the grain boundaries and Tb_2Fe_{17} phase is formed. However, the diffraction peak of Tb_2Fe_{17} phase cannot be detected, which may be due to the low content of this phase.

According to Table 1, the 2θ position of (110) peak of the alloys is fluctuant, which is attributed to the lattice distortion caused by mutual substitution of different elements in the alloys, thus resulting in diffraction peak shifting. Moreover, the lattice constant a of the alloys also fluctuates, whereas the I_{200}/I_{110} ratio exhibits converse tendency. The transmutation in lattice constant of the alloys is primarily pertinent to the substitution of Ga atoms in the lattice after the addition of Al atoms. An augmentation in the lattice constant of the alloys
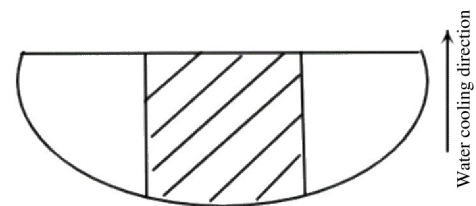

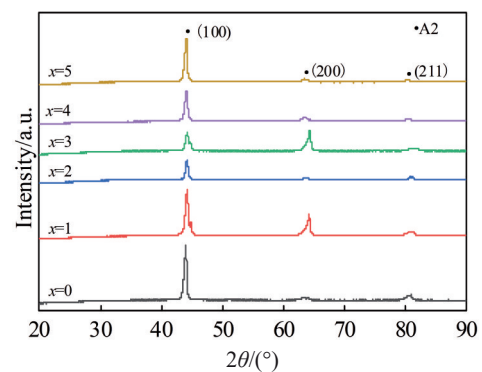Fig.1　Schematic diagram of sampling position of alloys

Fig.2　XRD patterns of $(Fe_{73}Ga_{27-x}Al_x)_{99.8}Tb_{0.2}$ (x=0, 1, 2, 3, 4, 5) alloys

Table 1   XRD analysis results of $(Fe_{73}Ga_{27-x}Al_x)_{99.8}Tb_{0.2}$ (x=0, 1, 2, 3, 4, 5) alloys

x	0	1	2	3	4	5
$2\theta_{100}$/(°)	44.03	44.20	44.17	44.25	44.08	44.08
a/nm	0.290 55	0.289 94	0.290 76	0.288 88	0.291 37	0.291 38
I_{200}/I_{110} ratio/%	3.0	42.5	10.0	86.6	8.6	10.6

indicates the decrease in lattice gap and vacancies in the alloy crystal. According to Ref. [25], vacancies can reduce the electron density in the surrounding area and improve the physical environment around Fe, hence enhancing the magnetostrictive properties of the alloys. The lattice constant of the alloys tends to increase, because the Al atomic radius is greater than the Ga atomic radius. When x=3, the lattice constant reaches the minimum value of 0.288 88 nm; the I_{200}/I_{110} ratio peaks at 86.6%, manifesting that (100) orientation in the alloys is enhanced, i.e., appropriate Al addition intensifies the (100) orientation. When the easy magnetization direction of Fe-Ga alloys is (100) direction, large magnetostriction can be achieved after the addition of Tb element.

2.2 Metallographic structure

Fig. 3 presents the metallographic structures of $(Fe_{73}Ga_{27-x}Al_x)_{99.8}Tb_{0.2}$ alloys. It can be seen that the alloys are mainly composed of cellular crystals and columnar dendrites. During the forced growth process of crystals, the interface is unstable, and the convex peaks and concave valley appear at the interface, resulting in the formation of cellular grains. The growth rate of the concave valley is slow, which is attributed to the accumulation of excess solute, thus inhibiting the growth process. The appearance of concave valley also triggers the additional protrusions in adjacent areas, which ultimately forms cellular structure through repeated processes. The development of columnar dendrite results from the enlargement of component supercooling zone, and the local bulge formed by the interface disturbance has larger extension in the solution. New component supercooling occurs, which destroys the stability of the original cellular crystal interface, changing the crystal growth direction towards the crystallography orientation with the fastest growth rate. At the same time, the cross section of the cellular crystal also shows lateral bulges, leading to the transformation from cellular crystal into columnar dendrites.

The grain structures in Fig. 3a and 3f mainly present irregular cellular shapes, whereas the grain structures in Fig. 3b and 3c are mainly composed of irregular cellular crystals and a small number of columnar dendrites. Fig. 3d shows columnar dendrites, and the grain structure in Fig.3e is composed of hexagonal cellular crystals. According to the liquid metal forming mechanism[26], with the gradual formation of dendrites, the liquid flow is less required during the final shrinkage stage of the solidification process, generating shrinkage porosity and porosity defects, which leads to the descent in the mechanical properties of alloys. This is consistent with the variation of hardness.

2.3 SEM and EDS analysis

Fig. 4 shows SEM images and EDS spectra of $(Fe_{73}Ga_{27-x}Al_x)_{99.8}Tb_{0.2}$ alloys. Table 2 shows EDS point analysis results of $(Fe_{73}Ga_{27-x}Al_x)_{99.8}Tb_{0.2}$ alloys. As shown in Fig.4, Tb element is enriched at the grain boundary, because the atom radius of Tb element is much larger than that of Fe and Ga elements and the Tb solubility in Fe-Ga solid solution remains low. In
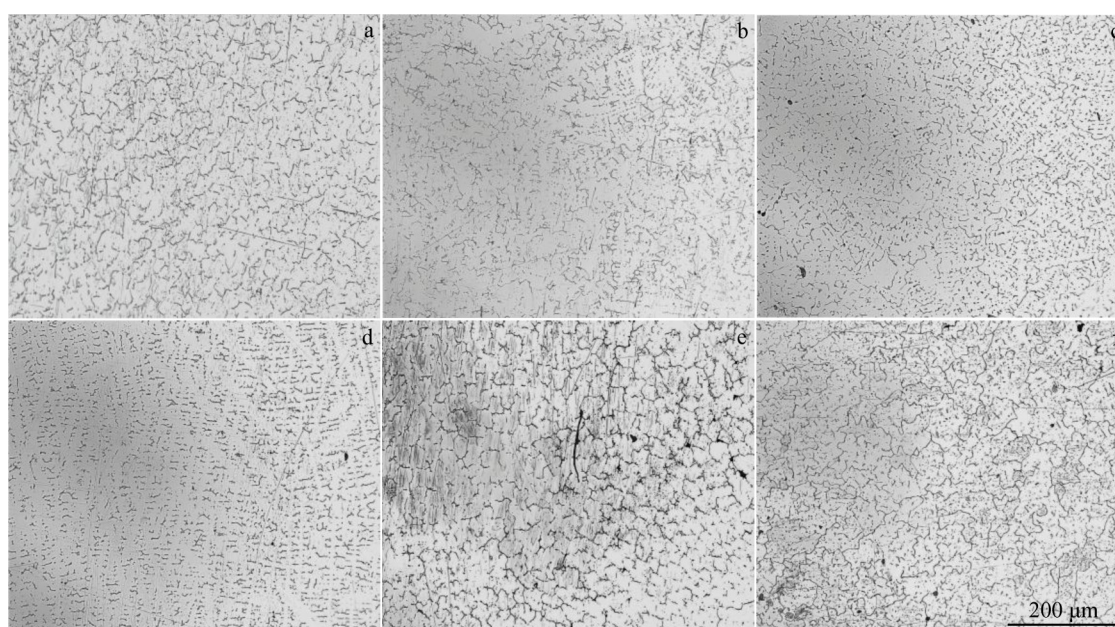

Fig.3   Metallographic structures of $(Fe_{73}Ga_{27-x}Al_x)_{99.8}Tb_{0.2}$ alloys: (a) x=0; (b) x=1; (c) x=2; (d) x=3; (e) x=4; (f) x=5
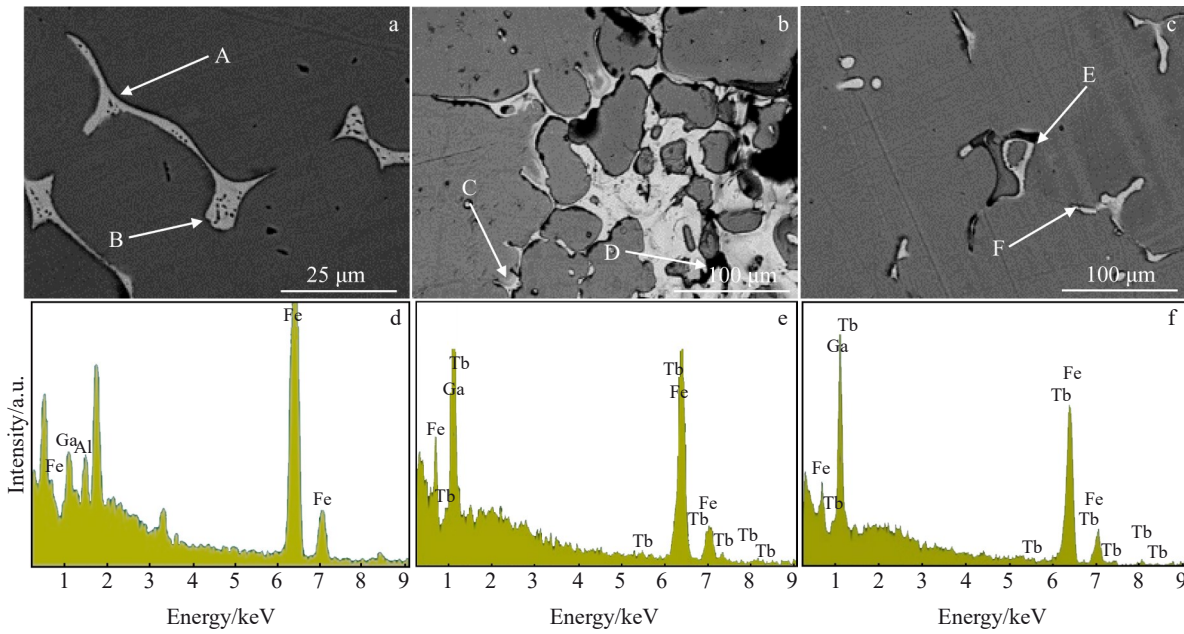
Fig.4　SEM images of $Fe_{73}Ga_{27-x}Al_x)_{99.8}Tb_{0.2}$ alloys with $x=0$ (a), $x=2$ (b), and $x=3$ (c); EDS spectra of point D (d), point E (e), and point F (f) in Fig.4a–4c

Ref.[27], when Tb element gathers at the grain boundaries, diverse compounds with Fe atoms, such as $TbFe_2$, $TbFe_3$, Tb_2Fe_{17}, and Tb_6Fe_{23}, may be generated, which significantly ameliorates the magnetostriction properties of the alloys.

According to EDS analysis results of point E and F in Table 2, the content ratios of Tb to Fe is 1: 8.67 and 1: 8.38, respectively, which are extremely close to the atom ratio of Tb and Fe in Tb_2Fe_{17} compound. Based on the abovementioned results, it can be inferred that Tb_2Fe_{17} phase, whose saturation magnetostrictive strain is more than 2.00×10^{-4}, is precipitated at the grain boundaries of $(Fe_{73}Ga_{24}Al_3)_{99.8}Tb_{0.2}$ alloy, which thereby increases the magnetostriction coefficient of the alloys. In addition, EDS analysis results of point D show that the Al content is relatively high, and it is far above the Al content in the nominal composition. The enrichment of Al element reinforces the pinning effect of the alloys, seriously impeding the magnetic domain rotation and thereby reducing the magnetostriction performance of the alloys.

2.4　Magnetostrictive properties

Fig.5 presents the relationships of parallel magnetostriction coefficients ($\lambda_{//}$) of $(Fe_{73}Ga_{27-x}Al_x)_{99.8}Tb_{0.2}$ alloys with magnetic field (H) and Al content. As shown in Fig.5a, the external magnetic field required for the $\lambda_{//}$ saturation after Tb addition

Table 2　EDS analysis results of marked points in Fig.4 (at%)

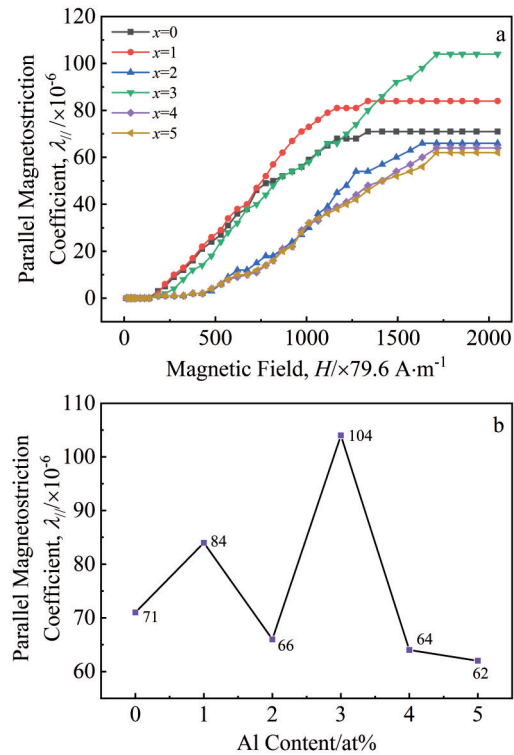| Point	Fe	Ga	Al	Tb
A	50.38	43.24	0.00	6.38
B	50.37	43.19	0.00	6.44
C	54.91	36.53	0.00	8.56
D	68.93	17.57	13.50	0.00
E	53.28	40.57	0.00	6.15
F	53.46	40.16	0.00	6.38

Fig.5　Relationships of parallel magnetostriction coefficients of $(Fe_{73}Ga_{27-x}Al_x)_{99.8}Tb_{0.2}$ alloys with magnetic field (a) and Al content (b)

is in the range of 103 480–135 320 A·m⁻¹. When the parallel magnetostrictive coefficient of the alloys reaches saturation, the required magnetic field becomes large with the increase in Al addition amount. Fig. 5b shows that the $\lambda_{//}$ value of $(Fe_{73}Ga_{27-x}Al_x)_{99.8}Tb_{0.2}$ alloys varies between 6.2×10^{-5} and

$1.04×10^{-4}$. Compared with that of alloy without Al addition, $\lambda_{//}$ value of the alloy with 1at% Al increases slightly. The decrease in lattice constant and the intensity enhancement of orientation [100] are conducive to the magnetostrictive properties of $(Fe_{73}Ga_{27-x}Al_x)_{99.8}Tb_{0.2}$ alloys. When Al content increases from 1at% to 2at%, the $\lambda_{//}$ value of the alloy decreases because Al element exists in the precipitate phase, which exerts pinning effect on the magnetic domains, therefore reducing the magnetoelastic property of the alloys[27]. The $\lambda_{//}$ value of alloy with 3at% Al reaches the maximum value of $1.04×10^{-4}$, which is related to the minimum lattice constant and the strongest intensity of orientation [100]. Tb_2Fe_{17} phase is beneficial to the improvement of magnetostrictive properties, and it is produced at the grain boundary of the alloys. The $\lambda_{//}$ value is decreased significantly when the Al content increases from 3at% to 5at%. Because the solid solution capacity of Fe and Al elements is more diminutive than that of Al and Ga elements, Al element destroys the Ga-Ga atomic pairs[28]. Clark et al[29] proposed that the Ga-Ga atomic pair was important for the large magnetostrictive properties of Fe-Ga alloys. Compared with that of $(Fe_{73}Ga_{27})_{99.8}Tb_{0.2}$ alloy, the $\lambda_{//}$ value of $(Fe_{73}Ga_{27-x}Al_x)_{99.8}Tb_{0.2}$ alloys with x=1 and 3 increases by 18.3% and 46.5%, respectively.

2.5 Hysteresis loop analysis

Fig. 6a shows the hysteresis loop diagram of $(Fe_{73}Ga_{27-x}Al_x)_{99.8}Tb_{0.2}$ alloys. Fig. 6b presents the results of saturation magnetization (M_s), remanent magnetization (M_r), and coercivity (H_c) of the $(Fe_{73}Ga_{27-x}Al_x)_{99.8}Tb_{0.2}$ alloys. According to Fig. 6a, the magnetization of all samples basically reaches the saturation state when the applied magnetic field approaches 1 T.

Fig. 6b shows that M_s of $(Fe_{73}Ga_{27-x}Al_x)_{99.8}Tb_{0.2}$ alloys fluctuates around $109.1±21.6$ A·m²·kg⁻¹. The M_r and H_c values of $(Fe_{73}Ga_{27-x}Al_x)_{99.8}Tb_{0.2}$ alloys change slightly around $0.3±0.9$ A·m²·kg⁻¹ and $(8.1±2.36)×10^{-4}$ T, respectively, and they both show the variation trend of decreasing, then increasing, and finally decreasing with the increase in Al content. However, M_s presents opposite variation trend. It is known that the materials with high M_s and low M_r values are able to save resources in the actual production, which is conducive to the development of products with light, thin, and short design and quick response to the inversion of the external magnetic field[30]. For soft magnetic materials, the lower H_c value indicates that they are susceptible to magnetization by external magnetic fields and are easily demagnetized by external magnetic fields or other elements, which reduces the hysteresis loss and magnetization power of materials and is beneficial to the practical application. According to the above analysis, the $(Fe_{73}Ga_{26}Al_1)_{99.8}Tb_{0.2}$ alloy possesses high M_s, low M_r, and low H_c, so it is more suitable for extensive production and application.

2.6 Room temperature stretching experiment

Fig. 7 shows the tensile strength and elongation results of $(Fe_{73}Ga_{27-x}Al_x)_{99.8}Tb_{0.2}$ alloys. As shown in Fig. 7a, the highest tensile strength of the alloys reaches 322.8 MPa at x=0. With
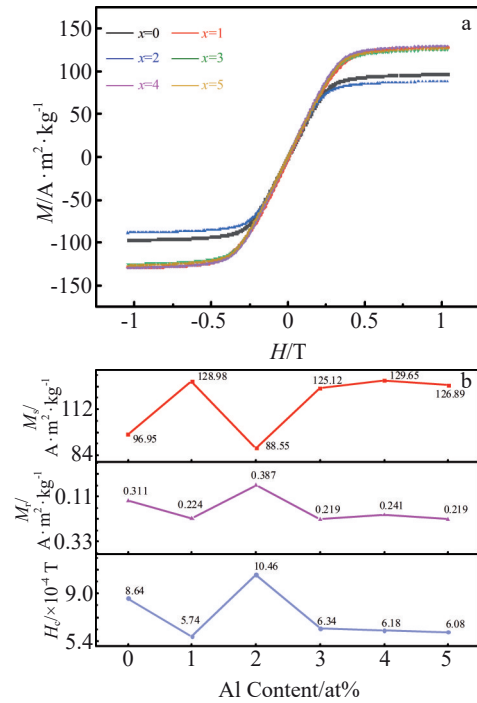
Fig.6 Hysteresis loop curves (a) and M_s, M_r, and H_c results (b) of $(Fe_{73}Ga_{27-x}Al_x)_{99.8}Tb_{0.2}$ (x=0, 1, 2, 3, 4, 5) alloys

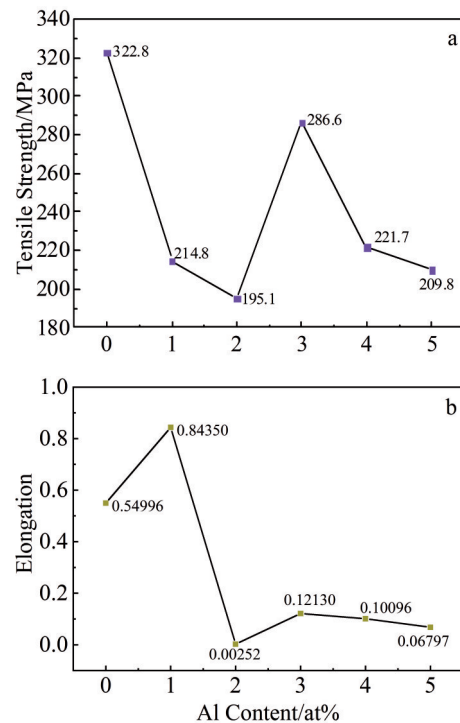Fig.7 Tensile strength (a) and elongation (b) of $(Fe_{73}Ga_{27-x}Al_x)_{99.8}$-$Tb_{0.2}$ (x=0, 1, 2, 3, 4, 5) alloys

the augmentation of Al atoms, the tensile strength of the alloys is decreased firstly, then increased, and decreased finally. Compared with that of $Fe_{73}Ga_{27}$ alloy, the tensile strength decreases after doping Tb element into the alloys. This is because the atomic radius of Tb is larger than that of Fe and Ga atoms and Tb element is enriched at the grain boundary,

thus increasing the tendency of grain boundary cracking. Fig. 7b shows that the elongation of $(Fe_{73}Ga_{26}Al_1)_{99.8}Tb_{0.2}$ alloy is greater than that of $(Fe_{73}Ga_{27})_{99.8}Tb_{0.2}$ alloy, suggesting that the addition of appropriate amount of Al element has a certain degree of improvement in plasticity. Compared with that of $(Fe_{73}Ga_{27})_{99.8}Tb_{0.2}$ alloy, the elongation of $(Fe_{73}Ga_{26}Al_1)_{99.8}Tb_{0.2}$ alloy increases by 53.4%.

2.7 Fracture morphology analysis

Fig. 8 shows the fracture morphologies of $(Fe_{73}Ga_{27-x}Al_x)_{99.8}Tb_{0.2}$ alloys. Point A and B in Fig. 8a are located at the white dots in the grain of $(Fe_{73}Ga_{27})_{99.8}Tb_{0.2}$ alloy and point C represents the white dot at the grain boundaries. EDS point analysis results are shown in Table 3. The Tb content is much higher in the grains and at the grain boundaries, compared with that in the matrix, proving that Tb element is segregated at grain boundaries or within the grains. Additionally, element segregation increases the fracture tendency along grain boundaries, so Tb element segregation is the principal reason for the fracture of $(Fe_{73}Ga_{27})_{99.8}Tb_{0.2}$ alloy. EDS analysis results of point D in Fig. 8b suggest that at the grain boundary of the $(Fe_{73}Ga_{26}Al_1)_{99.8}Tb_{0.2}$ alloy, the relative content of Al element is more than that in the nominal composition, indicating the Al segregation at the grain boundary, which dominates the alloy fracture. The fracture type of $(Fe_{73}Ga_{25}Al_2)_{99.8}Tb_{0.2}$ alloy is cleavage fracture. Apparent cleavage steps are usually composed of a sequence of diminutive fracture surfaces, which can be observed in Fig. 8h. The diminutive fracture surfaces at microlevel are usually represented by cleavage surfaces. For example, in a body-centered cubic (bcc) lattice of metals, the cleavage surfaces are mainly (001) crystal planes. Combined with XRD analysis results, the crystallography structure of $(Fe_{73}Ga_{25}Al_2)_{99.8}Tb_{0.2}$ alloy is

determined as α-Fe with bcc crystal structure, thus inferring that the cleavage plane of this group is primarily the (001) crystal plane. At point E, namely at the grain boundary, the Al element content is close to that in nominal composition. Based on the analysis results of point F, the Al element exsolution occurs at the cleavage step, primarily causing the cleavage fracture. The point G–I are located at the white dots on the fracture surface of the $(Fe_{73}Ga_{24}Al_3)_{99.8}Tb_{0.2}$ alloy. Their analysis results show that the Tb element content at point G and H is greater than that in the matrix phase, and the Al element content at point I is more than that in the matrix phase, indicating that the fracture is mainly caused by the segregation of Al and Tb elements.

The point J and K correspond to the white dots at the grain boundary and in the entire grain, respectively; the point L is located at the grain boundary. It can be seen that the relative content of Al element is larger than that in the matrix phase, indicating that the fracture of $(Fe_{73}Ga_{23}Al_4)_{99.8}Tb_{0.2}$ alloy is caused by the segregation of Al element at different positions. The point M and O are located at the white dots within the grain of $(Fe_{73}Ga_{22}Al_5)_{99.8}Tb_{0.2}$ alloy and the N point is located at the grain boundaries. It is demonstrated that the Tb element content at the M and O points is higher than that in the matrix, and the Al element content at the point O exceeds that in the matrix, implying that the fracture of $(Fe_{73}Ga_{22}Al_5)_{99.8}Tb_{0.2}$ alloy results from the Al segregation at the grain boundaries and the Tb segregation at grain boundaries or within grains.

In conclusion, the addition of Tb element increases the crack tendency of the alloys. The fracture mechanisms of $(Fe_{73}Ga_{27-x}Al_x)_{99.8}Tb_{0.2}$ alloys include the single element segregation of Al element and Tb element, the segregation of multiple elements at different positions, and Al element
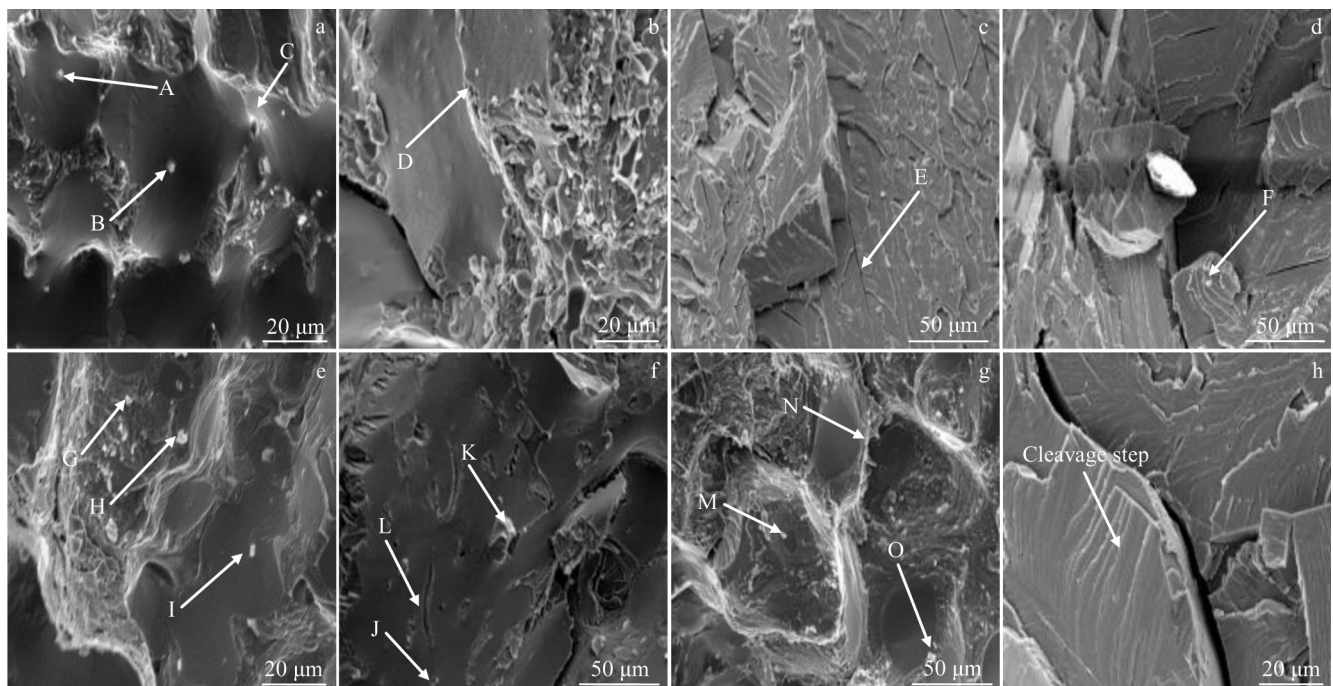

Fig.8　Fracture morphologies of $(Fe_{73}Ga_{27-x}Al_x)_{99.8}Tb_{0.2}$ alloys: (a) *x*=0; (b) *x*=1; (c–d, h) *x*=2; (e) *x*=3; (f) *x*=4; (g) *x*=5

Table 3 EDS analysis results of marked points at fracture region of $(Fe_{73}Ga_{27-x}Al_x)_{99.8}Tb_{0.2}$ alloys in Fig.8 (at%)

Point	Fe	Ga	Al	Tb
A	63.45	26.54	0.00	10.01
B	65.93	23.71	0.00	10.36
C	64.25	33.21	0.00	2.54
D	65.71	31.18	3.11	0.00
E	79.02	19.06	1.92	0.00
F	0.00	0.00	100.00	0.00
G	50.86	40.58	2.27	6.29
H	47.31	41.71	4.08	6.90
I	33.35	7.80	58.85	0.00
J	57.22	20.58	22.20	0.00
K	62.74	21.61	15.65	0.00
L	55.71	25.33	18.96	0.00
M	47.60	38.86	7.11	6.43
N	68.87	23.92	7.21	0.00
O	49.14	38.53	5.96	6.37

exsolution.

2.8 Vickers hardness

Fig. 9 presents the Vickers hardness of the $(Fe_{73}Ga_{27-x}Al_x)_{99.8}Tb_{0.2}$ (x=0, 1, 2, 3, 4, 5) alloys. The hardness is gradually decreased with the increase in Al content from 0at% to 3at% . Besides, the number of irregular cellular crystals reduces and they are gradually transformed into columnar dendrites. In Ref. [31], because of the presence of dendritic crystals, the liquid flow during the final shrinkage process of the alloys in the solidification stage is insufficient, defects, such as shrinkage pores and shrinkage cavities, are formed, thus degrading the mechanical properties of the alloys. The hardness decreases in this stage, which may be influenced by the columnar dendritic crystals. The maximum Vickers hardness of 3331.80 MPa can be obtained at x=4, which is attributed to the evolution of small hexagonal cellular crystal structures. The Vickers hardness of $(Fe_{73}Ga_{23}Al_4)_{99.8}Tb_{0.2}$ alloy (3331.80 MPa) increases by 8.2%, compared with that of $(Fe_{73}Ga_{27})_{99.8}Tb_{0.2}$ alloy. Furthermore, when x=1, 2, 3, 5, the hardness values of $(Fe_{73}Ga_{27-x}Al_x)_{99.8}Tb_{0.2}$ alloys are all lower

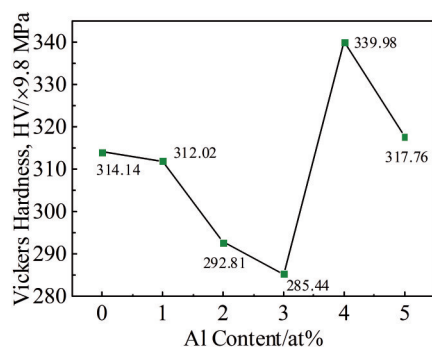Fig.9 Vickers hardness of $(Fe_{73}Ga_{27-x}Al_x)_{99.8}Tb_{0.2}$ (x=0, 1, 2, 3, 4, 5) alloys

than that with x=4. This may be related to the enrichment of Tb element at the grain boundaries, which commonly leads to the degradation of mechanical properties of the alloys.

3 Conclusions

1) The addition of Al element does not change the phase structure of $(Fe_{73}Ga_{27})_{99.8}Tb_{0.2}$ alloy and $(Fe_{73}Ga_{27-x}Al_x)_{99.8}Tb_{0.2}$ alloy is still composed of A2 phase and Tb_2Fe_{17} phase. The grain shape of the alloys preeminently affects the hardness of $(Fe_{73}Ga_{27-x}Al_x)_{99.8}Tb_{0.2}$ alloys, and the alloys are mainly composed of cellular crystals and columnar dendrites.

2) Compared with that of $(Fe_{73}Ga_{27})_{99.8}Tb_{0.2}$ alloy, the $\lambda_{//}$ value of $(Fe_{73}Ga_{27-x}Al_x)_{99.8}Tb_{0.2}$ alloys with x=1 and 3 increases by 18.3% and 46.5%, respectively, which is mainly related to the decrease in lattice constant, the enhancement of (100) orientation intensity, and the formation of Tb_2Fe_{17} phase. $(Fe_{73}Ga_{26}Al_1)_{99.8}Tb_{0.2}$ alloy has the characteristics of high M_s, low M_r, and low H_c, which can save resources in actual manufacture and reduce production cost.

3) At room temperature, the tensile strength of $(Fe_{73}Ga_{27})_{99.8}Tb_{0.2}$ alloy can reach 322.8 MPa, and it decreases after adding Al element. Compared with that of $(Fe_{73}Ga_{27})_{99.8}Tb_{0.2}$ alloy, the elongation of $(Fe_{73}Ga_{26}Al_1)_{99.8}Tb_{0.2}$ alloy increases by 53.4%. The fracture mechanisms for $(Fe_{73}Ga_{27-x}Al_x)_{99.8}Tb_{0.2}$ alloys include intergranular brittle fracture and cleavage fracture, which results from the segregation of Ga, Tb, and Fe elements. At x=4, the Vickers hardness of the alloys achieves 3331.80 MPa, which increases by 8.2% compared with that of $(Fe_{73}Ga_{27})_{99.8}Tb_{0.2}$ alloy.

References

1 Liu H F, Lim C W, Gao S *et al. Mechatronics*[J], 2019, 57: 20

2 Qiao R H, Gou J M, Yang T Z *et al. Journal of Materials Science & Technology*[J], 2021, 84(25): 173

3 Wang N J, Liu Y, Zhang H W *et al. China Foundry*[J], 2016, 13(2): 75

4 Zhou Z G, Li J H, Bao X Q *et al. Journal of Alloys and Compounds*[J], 2020, 826: 153959

5 Clark A E, Restorff J B, Wun-Fogle M *et al. IEEE Transactions on Magnetics*[J], 2000, 36(51): 3238

6 Kellogg R A, Flatau A B, Clark A E *et al. Journal of Applied Physics*[J], 2002, 91(10): 7821

7 Yao Zhanquan, Tian Xiao, Hao Hongbo *et al. Rare Metal Materials and Engineering*[J], 2016, 45(7): 1777 (in Chinese)

8 Mungsantisuk P, Corson R P, Guruswamy S. *Journal of Applied Physics*[J], 2005, 98(12): 123907

9 Srisukhumbowornchai N, Guruswamy S. *Journal of Applied Physics*[J], 2001, 90(11): 5680

10 Zhou Y, Wang B W, Li S Y *et al. International Journal of Materials Research*[J], 2008, 99(3): 251

11 Zhou Y, Wang X L, Wang B W *et al. Journal of Applied Physics*[J], 2012, 111(7): 07A332

12 Li M M, Li J H, Bao X Q *et al. Applied Physics Letters*[J], 2017,

111(4): 042403

13　Li X L, Bao X Q, Liu Y Y *et al. Applied Physics Letters*[J], 2017, 111(16): 162402

14　Liu Y Y, Li J H, Gao X X. *Journal of Magnetism and Magnetic Materials*[J], 2017, 423(1): 245

15　Nolting A E, Summers E. *Journal of Materials Science*[J], 2015, 50(15): 5136

16　Emdadi A, Palacheva V V, Cheverikin V V *et al. Journal of Alloys and Compounds*[J], 2018, 758: 214

17　Jiang Liping, Zhang Guangrui, Hao Hongbo *et al. Transactions of Materials and Heat Treatment*[J], 2012, 33(5): 44 (in Chinese)

18　He Y K, Ke X Q, Jiang C B *et al. Advanced Functional Materials*[J], 2018, 28(20): 20

19　Wang Rui, Tian Xiao, Yao Zhanquan *et al. Chinese Rare Earths*[J], 2020, 41(2): 24 (in Chinese)

20　Zhang Guangrui, Jiang Liping, Hao Hongbo *et al. Chinese Rare Earths*[J], 2013, 34(3): 32 (in Chinese)

21　Meng C Z, Wang H, Wu Y Y *et al. Scientific Reports*[J], 2016, 6: 34258

22　Meng C H, Wu Y Y, Jiang C B. *Materials & Design*[J], 2017,

130: 183

23　Wu Y Y, Fang L, Meng C Z *et al. Materials Research Letters*[J], 2018, 6(6): 327

24　Meng C, Jiang C. *Scripta Materialia*[J], 2016, 114(15): 9

25　Li Jiheng, Gao Xuexu, Zhu Jie *et al. Chinese Journal of Rare Metals*[J], 2017, 41(2): 155 (in Chinese)

26　Dai Binyu. *Liquid Metal Forming Theory*[M]. Beijing: National Defense Industry Press, 2010: 53 (in Chinese)

27　Basumatary H, Palit M, Arout C J *et al. Scripta Materialia*[J], 2008, 59(8): 878

28　Zhang J J, Ma T Y, Yan M. *Physica B: Condensed Matter*[J], 2009, 404(21): 4155

29　Clark A E, Wun-Fogle M, Restorff J B *et al. IEEE Transactions on Magnetics*[J], 2001, 37(41): 2678

30　Yan Mi, Peng Xiaoling. *Fundamentals of Magnetism and Magnetic Materials*[M]. Hangzhou: Zhejiang University Press, 2006 (in Chinese)

31　Yu Yongning. *Principle of Metal*[M]. Beijing: Metallurgical Industry Press, 2003 (in Chinese)

Al元素添加对(Fe$_{73}$Ga$_{27}$)$_{99.8}$Tb$_{0.2}$合金微观结构、磁性能及力学性能的影响

杜金超[1,2]，李小飞[1]，焦佩英[1]，张志广[1]，龚　沛[1]

(1. 内蒙古工业大学　材料科学与工程学院，内蒙古　呼和浩特　010051)

(2. 钢铁研究总院　功能材料研究所，北京　100081)

摘　要：通过真空电弧炉制备(Fe$_{73}$Ga$_{27-x}$Al$_x$)$_{99.8}$Tb$_{0.2}$（x=0，1，2，3，4，5）合金，研究Al添加对合金的微观结构、磁性能和力学性能的影响。结果显示，合金的相结构仍为A2相和Tb$_2$Fe$_{17}$相，其金相组织由胞状晶和柱状树枝晶组织组成。合金的晶格常数降低、(100)取向性增强以及晶界处的Tb$_2$Fe$_{17}$相对磁致伸缩性能有显著影响。合金的断口形貌为沿晶脆性断裂和解理断裂，产生断裂的原因包括Tb和Al元素偏析。(Fe$_{73}$Ga$_{24}$Al$_3$)$_{99.8}$Tb$_{0.2}$合金的平行磁致伸缩应变（$\lambda_{//}$）最高达到1.04×10^{-4}。值得注意的是，相比于(Fe$_{73}$Ga$_{27}$)$_{99.8}$Tb$_{0.2}$合金，(Fe$_{73}$Ga$_{26}$Al$_1$)$_{99.8}$Tb$_{0.2}$合金的$\lambda_{//}$提高了18.3%，伸长率提高了53.4%，并且(Fe$_{73}$Ga$_{26}$Al$_1$)$_{99.8}$Tb$_{0.2}$合金兼具高饱和磁化强度（M_s）、低剩余磁化强度（M_r）和矫顽力（H_c）等特性，在实际生产中可以降低生产成本，但该合金的抗拉伸强度和维氏硬度有所下降。因此，研究Al元素添加对Fe-Ga合金的微观机理对开发Fe-Ga合金器件具有重要意义。

关键词：(Fe$_{73}$Ga$_{27}$)$_{99.8}$Tb$_{0.2}$合金；Al掺杂；微观结构；磁性能；力学性能

作者简介：杜金超，男，1998年生，硕士生，内蒙古工业大学材料科学与工程学院，内蒙古　呼和浩特　010051，E-mail：20201100236@imut.edu.cn